Experimental assessment of an End Notched Flexure test configuration with an inserted roller for analyzing mixed-mode I/II fracture toughness

A. Boyano*[a], J. De Gracia[a], A. Arrese[b], F. Mujika[b]

[a,b] Materials + Technologies Group, Department of Mechanical Engineering
[a] The University College of Engineering of Vitoria-Gasteiz, University of the Basque Country (UPV/EHU)
Nieves Cano, 12, 01006 Vitoria-Gasteiz, Spain
*e-mail: ana.boyano@ehu.eus // Tel: +34 945 013933
[b] Engineering College of Gipuzkoa - University of the Basque Country (UPV/EHU)
Plaza de Europa, 1, 20018 San Sebastian, Spain

Abstract

This study describes the experimental work related to a test configuration proposed recently, based on an End Notched Flexure test configuration modified with an inserted roller. Various mixed-mode ratio tests have been performed by the variation of the radius or the position of the inserted roller. The crack length during propagation is determined without any optical measurement, based on the experimental compliance of the specimen. Consequently, energy release rate curves have been obtained at each point during the test. As the mixed mode varies during the test, the linear fracture criterion has been used for fitting experimental data of different specimens at different test conditions. The values of G_{Ic} and G_{IIc} obtained after that data fitting agreed with those obtained from pure mode tests.

Keywords: Interlaminar failure; Mixed-mode; Fracture toughness; Test method.

1   INTRODUCTION

Delamination, or interlaminar fracture, is a major failure mode for fibre-reinforced composite laminates [1-4]. It usually grows under the combination of modes I and II [5,6]. It is characterised by the energy required to create a new fracture surface per unit surface area, namely interlaminar fracture toughness [2,7-9].

Extensive experiments have been conducted to investigate the mixed-mode fracture of composite laminates using different type of test configurations, as was reviewed by Brunner et al [10], such as Mixed Mode Bending test (MMB) [11-14], Asymmetric Double Cantilever Beam (ADCB) test [15,16], Single-Leg Four Point Bending test (SLFPB) [17] and Compact Tension Shear specimen (CTS) [18]. Bennatti et al [19] developed an enhanced beam-theory model of the MMB test, after a review of the existing models. They deduced a complete explicit solution for unidirectional and multidirectional laminated specimens, as well as for adhesively bonded specimens.

The mixed-mode fracture tests are used not only in laminated composites: They have also a wide application for studying fracture in wood [20-23] , in adhesively bonded joints [24-26], or even analysing bones [27].

One of the critical issues of this type of test is the crack length determination [28-30]. The lack of accuracy when determining the crack length could affect to the value of fracture toughness [12,28]. Related to this aspect, it is important to determine the value of the crack length during the propagation, not only to define the energy release rate curves as a function of the crack advance, but also for analyzing the propagation failure envelope [31]. Moreover the toughness contour, in which fracture toughness is plotted as a function of mode mixtures, is useful for establishing failure criterion used in damage tolerance analyses of composite structures [32]. In the formulation of a fracture criterion it is necessary to take the fracture toughness recorded at some mixed-mode ratios as reference [33-37].

The present study deals with the experimental work concerning a test configuration proposed recently [38]. That configuration is an ENF test with an inserted roller for promoting mixed mode I/II. Therefore, it will be referred as ENFR. The aim of the present study is to apply that methodology to different experimental conditions, to obtain crack length without optical determination of crack tip position and to use the results during crack propagation in order to determine G_{Ic} and G_{IIc} and to compare them to the ones obtained in the pure mode tests.

NOMENCLATURE

$a, a_i, \Delta a$	Crack length, corrected crack length and crack increment, respectively
c_0, c_i	Distances from the support to the position of the roller when it is at the outer side and at the inner side of the support, respectively
$b, 2h$	Width and thickness of the specimen, respectively
C_{spec}, C_s, C_{exp}	Compliance of the specimen, of the system and experimental compliance, respectively
$C_{outer\,side}, C_{inner\,side}, C_{c=0}$	Analytic compliance when the roller is located at the outer side of the support, at the inner side and above the support, respectively.
k_S	Stiffness of the system
δ_0, P_0	Initial displacement and initial load, respectively
δ	Displacement of the middle point of the specimen
$\delta_{spec}, \delta_{expc}$	Calculated and experimental displacement of the middle point of the specimen, respectively
E_f	Flexural modulus
$G_{LT}, G_{LT'}$	In-plane shear modulus and out of plane shear modulus, respectively
G_I, G_{II}, G	Energy Release Rates for mode I, mode II, and total, respectively
L	Half span of the test
P	Applied Load
R	Roller radius
R^2	R squared parameter
G_{Ic}	Critical fracture toughness of mode I
G_{IIc}	Critical fracture toughness of mode II
G_{II}^0	Normalized G_{II} with respect to the critical value
G_I^0	Normalized G_I with respect to the critical value

2 ANALYTICAL BACKGROUND

The test configuration is based on the ENF test. In order to get mixed mode, a roller is introduced between the two surfaces of the crack: The mode II is provided by the external load and the mode I is obtained by the opening of the crack due to the insertion of the roller as shown in Fig. 1. The roller can be located at the outer side or at the inner side of the support. The analytic approach of the test configuration has been carried out in a previous study and it has been checked with numerical results obtained by FEM [38].
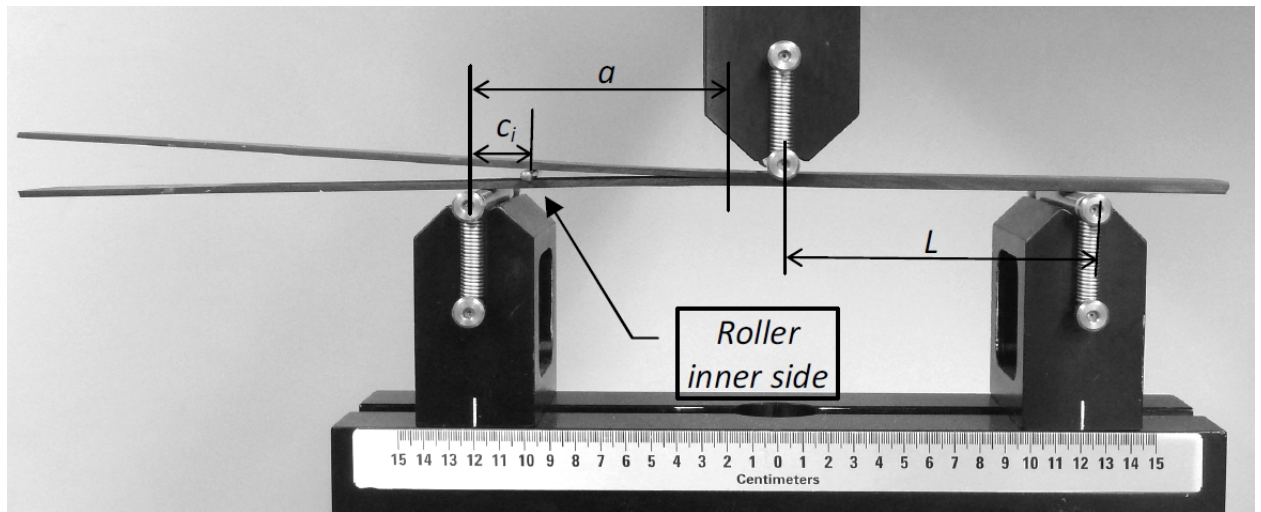

Fig. 1 Test configuration with the roller located at the inner side

Due to the roller introduction, there is an initial negative displacement without load, called δ_0. Furthermore, when the displacement is zero, there is a positive load, called P_0, as shown in Fig. 2.
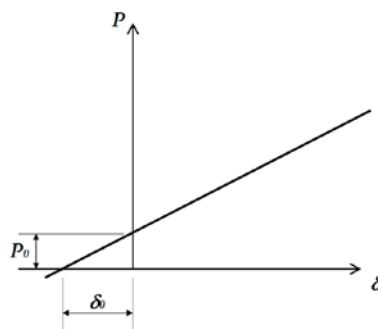

Fig. 2 Theoretical load-displacement curve

The compliance of this test is given by:

$$C = \frac{\delta}{P - P_0} = \frac{-\delta_0}{P_0} = \frac{\delta - \delta_0}{P} \tag{1}$$

In spite of bending and shear effects have been included in the analytic approach, in the present section the main results contain bending effects, for the sake of simplicity. Nevertheless, the calculations concerning the experimental part have been carried out including also shear effects. The analytic compliance for the three positions of the roller, can be expressed as follows [38]:

$$C_{outer\ side} = \frac{1}{8E_f bh^3}\left[\frac{(a-c_o)^3(3a^3+3ac_o^2+c_o^3)}{a^3}+2L^3\right]$$

$$C_{inner\ side} = \frac{3a^3+2L^3+c_i^3+3ac_i^2}{8E_f bh^3}$$

$$C_{c=0} = \frac{3a^3+2L^3}{8E_f bh^3}$$

(2)

The energy release rate due to each mode contribution is given by:

$$\text{Outer side}\quad G_I = \frac{3R^2Eh^3}{4a^4}-\frac{3PRc_o(a^2-c_o^2)}{4a^4b}+\frac{3P^2c_o^2(a^2-c_o^2)^2}{16a^4E_f b^2h^3}\qquad G_{II}=\frac{9P^2(a-c_o)^2}{16E_f b^2h^3}$$

$$\text{Inner side}\quad G_I = \frac{3R^2E_f h^3}{4(a-c_i)^4}+\frac{3PRc_i}{4b(a-c_i)^2}+\frac{3P^2c_i^2}{16E_f b^2h^3}\qquad G_{II}=\frac{9P^2a^2}{16E_f b^2h^3}$$

$$c=0\qquad\qquad G_I=\frac{3R^2E_f h^3}{4a^4}\qquad\qquad G_{II}=\frac{9P^2a^2}{16E_f b^2h^3}$$

(3)

It is worth remembering that when the roller is positioned at the outer side, the value (a-c_o) is the usual crack length measured in the ENF test configuration, as it can be seen in Fig. 3.
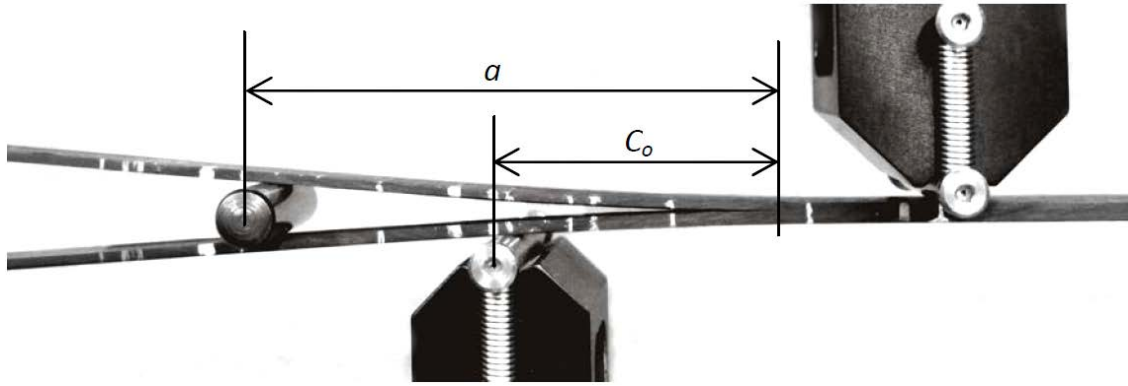

Fig. 3 Roller positioned at the outer side

Furthermore, in order to take into account the effect of rotation of the crack arms at the crack tip when G_I is determined, the crack length must be corrected. The effect of the end rotation could be modelled by increasing the real length by an amount Δa given by [38,39]:

$$\frac{\Delta a}{h} = \sqrt{\frac{E_L}{11G_{LT}}\left[3-2\left(\frac{\Gamma}{1+\Gamma}\right)^2\right]}\qquad \Gamma = 1.18\frac{\sqrt{E_L E_T}}{G_{LT}}$$

(4)

Thus, the crack length used in the expression for G_I has been corrected weighting the contribution of mode I according to:

$$a_I = a + \frac{G_I}{G} \Delta a \qquad (5)$$

3   EXPERIMENTAL

3.1   Materials, test apparatus and procedure

T6T/F593 prepregs provided by Hexcel Composites with a 55% volume-content of fiber were used to produce laminates. The plates were manufactured by hot press molding. Sixteen-layered unidirectional laminates, $[0]_{16}$, were made with a Teflon film introduced centered during the piling up process in order to make the initial crack. The specimens were cut with a diamond disc saw, being the nominal thickness and width 3 mm and 15 mm, respectively. The edges of the laminate were discarded for the preparation of the specimens. Tests were performed on an MTS-Insight 100 electromechanical testing machine equipped with a 5kN load cell, operating in a displacement controlled mode. In order to avoid the influence of the resin rich area the specimens were precracked in mode II by a ENF test, increasing the cracked length around 5 mm.

3.2   Determination of elastic parameters

All the specimens were tested using a procedure based on three-point bending tests at five different spans proposed by Mujika[40], in order to obtain the flexural modulus, E_f and the out of plane shear modulus $G_{LT'}$, which is equal to the in-of-plane shear modulus G_{LT} assuming that the material is transversely isotropic.

In order to analyze the system stiffness k_S, a specimen placed on a thick steel block was tested five times as shown in Fig. 4. The average value obtained for the stiffness of the system was k_s = 24 kN/mm.
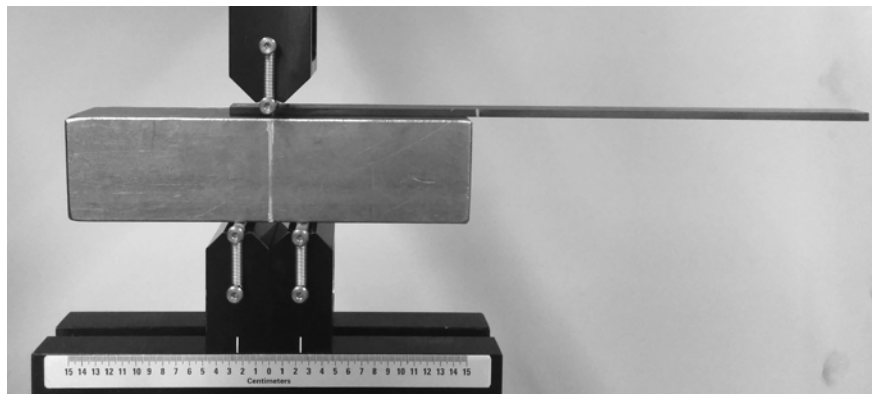

Fig. 4 Test for obtaining system stiffness

The experimental displacement (δ_{exp}) is the addition of the specimen displacement (δ_{spec}) and the displacement due to the system compliance $C_s = k_s^{-1}$. Then, the compliance of the specimen is given by:

$$C_{spec} = C_{exp} - C_s \tag{6}$$

Flexural tests were carried out in the un-cracked zone, without the roller, as shown in Fig. 5 (a) and (b) for spans (mm) 70, 80, 90, 100 and 120. The mean values corresponding to five specimens were:

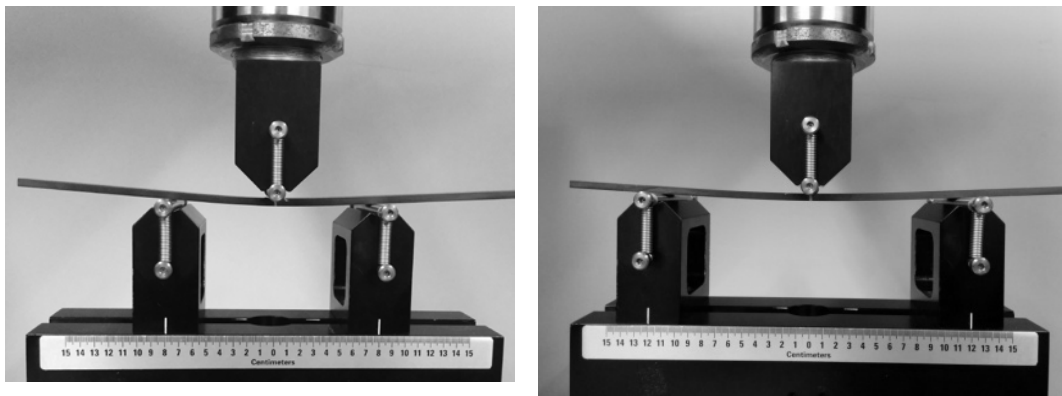E_f = 107.4 (±1.4) GPa

$G_{LT'}$ = 4.3 (±0.4) GPa

Fig. 5 Flexural tests: a/ Span 80 mm; b/ Span 120 mm

In order to obtain experimentally the load-displacement curve of Fig. 2 with initial conditions, the experimental displacement is defined as 0 when the contact between the load nose and the specimen without roller occurs, as it is shown in Fig. 6. After inserting the roller, there is an initial negative displacement δ_0 for the zero load condition. Actually, the contact in the testing machine has been defined when the load was 0.5 N.
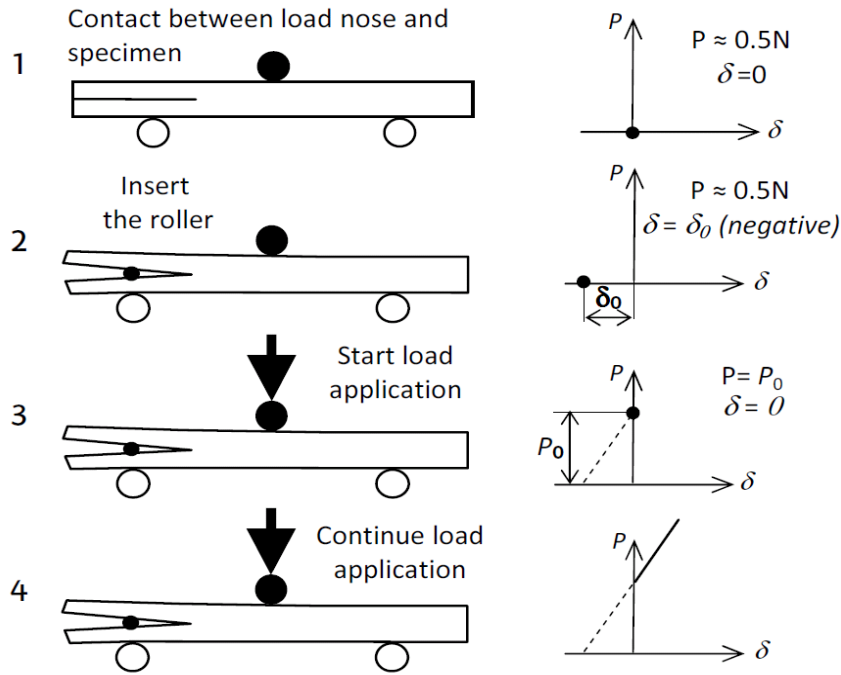
Fig. 6 Initial Conditions in Load-Displacement graph

Therefore, the experimental compliance at each point of the test is:

$$C_{exp} = \frac{\delta_{exp} - \delta_0}{P} \qquad (7)$$

According to Eq. (6) the compliance of the specimen leads to:

$$C_{spec} = \frac{\delta_{exp} - \delta_0}{P} - C_s \qquad (8)$$

3.3   Crack length determination without optical measurements

One of the critical issues of the fracture tests is the difficulty of monitoring the crack length during its propagation, especially when mode II loading predominates [28-30,41]. One of the objectives of the present study is the determination of the crack length without optical determination of the crack tip position. The determination of the crack length is based on the variation of the compliance during the crack advance, based on the work of Arrese et al [42] developed for the ENF test.

To determine the crack length from the experimental data, it is necessary to isolate it from the corresponding equation that includes the elastic properties of the material, Eq. (2). Regarding the particular case in which the roller is positioned above the support, that is $c = 0$, isolating the crack length is possible. However, when $c \neq 0$ it is not possible to obtain an explicit expression of the crack length. In those cases, the crack length at each point of the test is determined seeking for the value of a which satisfies that theoretical compliance given in Eq.(2) is equal to the specimen compliance given in (8), as it is shown in Fig. 7. This procedure gives the crack length at each point during the test.
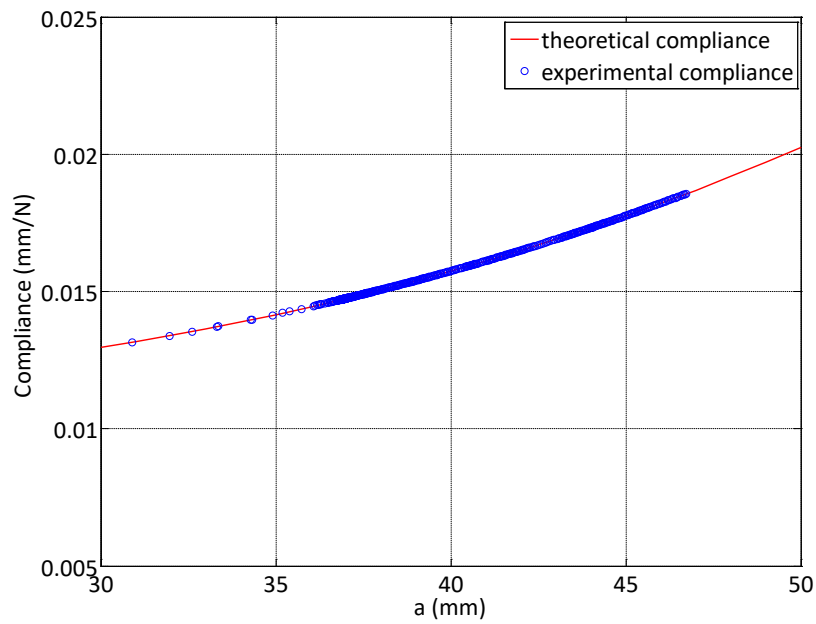
Fig. 7 Theoretical and experimental compliance in a mixed mode test

In order to asses the suitability of crack length measurement for the mixed mode specimen, ENF test measurements were performed considering the "Beam Theory including Bending Rotation effects" (BTBR) method presented by Arrese et al. as a verification method. For the mixed mode tests, the bending rotation effects were not included, because the support roller radii were 2.5mm and thus the influence was negligible [42]. This fact is shown in Fig. 8, where before the compliance increasing due to propagation, the compliance remains constant, without any reduction associated to the effect of contact change between specimen and supports.
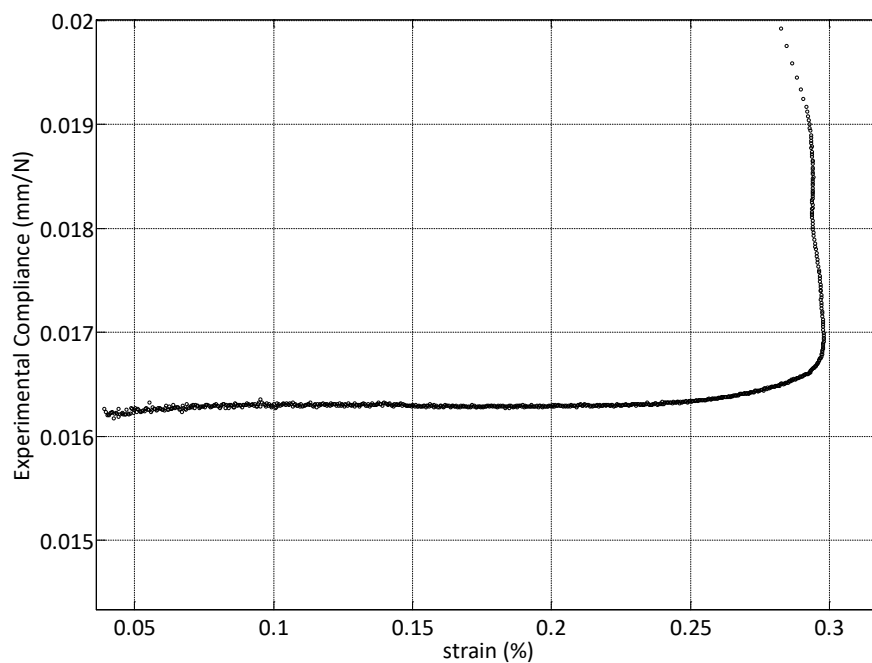
The steps of the experimental procedure are explained in Fig. 9.

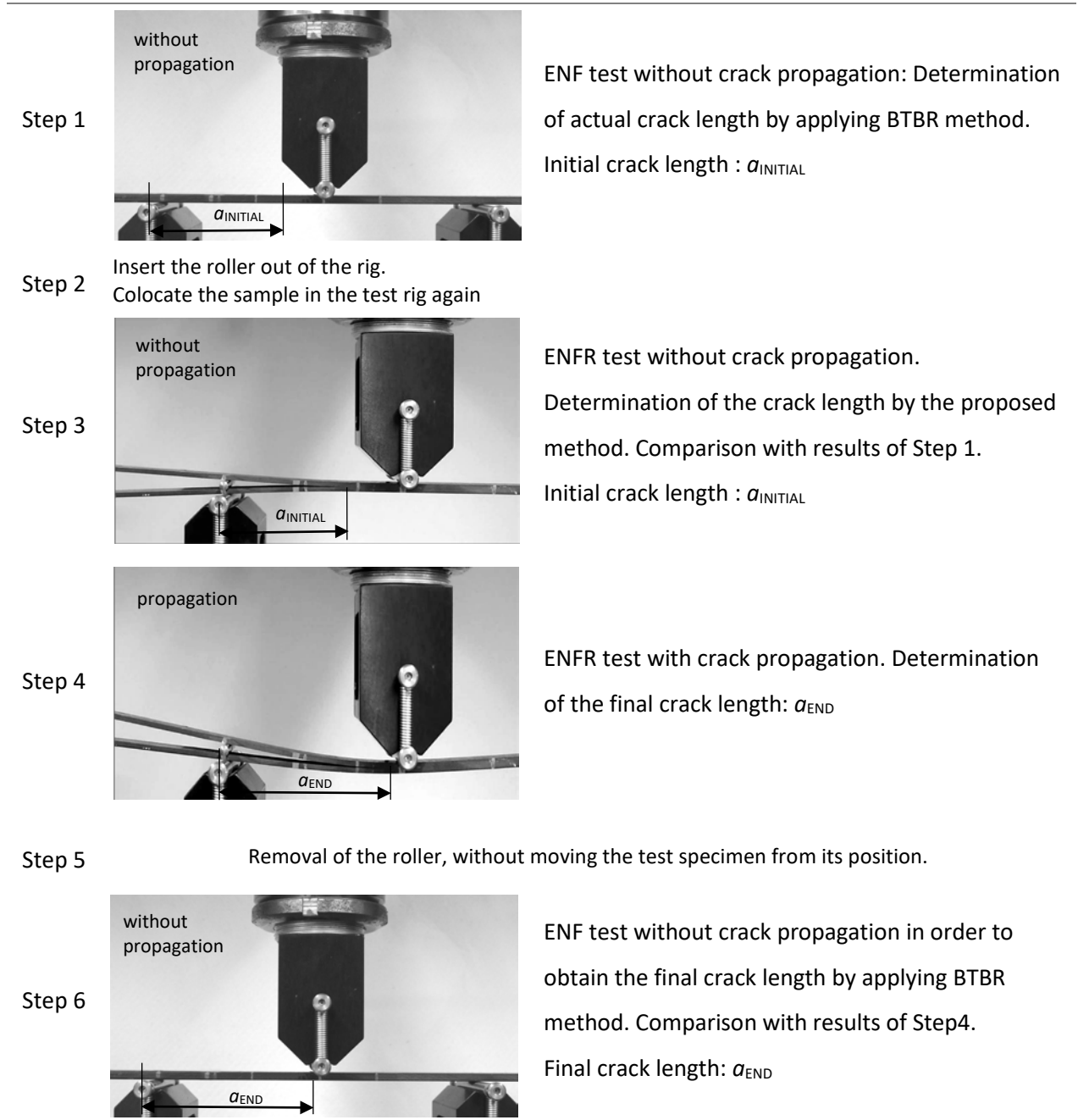|		
Step 1		ENF test without crack propagation: Determination of actual crack length by applying BTBR method. Initial crack length : $a_{INITIAL}$
Step 2	Insert the roller out of the rig. Colocate the sample in the test rig again	
Step 3		ENFR test without crack propagation. Determination of the crack length by the proposed method. Comparison with results of Step 1. Initial crack length : $a_{INITIAL}$
Step 4		ENFR test with crack propagation. Determination of the final crack length: a_{END}
Step 5	Removal of the roller, without moving the test specimen from its position.	
Step 6		ENF test without crack propagation in order to obtain the final crack length by applying BTBR method. Comparison with results of Step4. Final crack length: a_{END}

Fig. 9. Experimental procedure for crack measurement assesment.

The nomenclature that has been used in order to identify each specimen and test condition is ai-Rj-ck. Where ai is the nominal initial crack length; Rj is the inserted roller radius; and ck is the value of the c

distance that defines the position of the roller. This distance is positive when the roller is at the inner side and negative when it is at the outer side. For instance, a40-R1-c8 is the test with initial nominal crack length of 40 mm, an inserted roller of 1mm radius and positioned at 8mm at the inner side of the support.

The results of the crack length measurement are presented in Table 1 and Table 2. As it can be seen in Table 1 for the same roller radius R=1 mm, three positions of the roller have been analyzed. Comparing the results of ENF test without crack propagation (Step 1) and results of the initial value of the crack length of mixed mode tests (Step 3), the maximum error is 0.7 mm, less than 2%. This difference could be related to the fact that the test sample is removed from the test rig in order to insert the roller (Step 2), and one can not assure exactly the same position when returning it to the test fixture, in spite of there are marks on the sample.

Otherwise after the mixed mode tests (Step 4), the roller can be removed from the specimen by hand without moving it (Step 5), just applying a small load by means of the test machine. Therefore, the last crack length measured at Step 4 should be the same as the one measured at Step 6, being marked in bold text in Table 1 and in Table 2. In this case, the maximum error is 0.4 mm, which is less than 1%.

Table 1 Results for crack measurement changing the position of the roller

TEST DATA	STEP	TEST TYPE	$a_{INITIAL}$ (mm)	a_{END} (mm)
a40-R1-c0	Step 1	ENF without	40.4	
	Step 3	ENFR without	40.4	
	Step 4	ENFR propag	40.4	**47.1**
	Step 6	ENF without	**47.0**	
a40-R1-c5	Step 1	ENF without	39.3	
	Step 3	ENFR without	39.8	
	Step 4	ENFR propag	39.8	**45.2**
	Step 6	ENF without	**45.3**	
a30-R1-c8	Step 1	ENF without	30.5	
	Step 3	ENFR without	30.2	
	Step 4	ENFR propag	30.2	**35.1**
	Step 6	ENF without	**35.5**	

In Table 2 the position of the roller is fixed at c=0 mm (above the support), and three different radii have been studied. Comparing results of Step 1 and Step-3, the maximum error is 0.8 mm, less than 2%. Regarding the final value of the crack length, the maximum error in this case is 1.4mm, less than 3%.

It can be concluded that the crack length can be determined without optical methods, which is one of the most important drawbacks for any test that includes mode II, according to the analysis carried out by Szekrényes for the particular configuration corresponding to c=0 [29].

Table 2 Results for crack measurement changing the radius of the roller

TEST DATA	STEP	TEST TYPE	$a_{INITIAL}$ (mm)	a_{END} (mm)
a40-R0.5-c0	Step 1	ENF without	39.8	
	Step 3	ENFR without	39.8	
	Step 4	ENFR propag	39.8	**58.7**
	Step 6	ENF without	**58.8**	
a44-R0.9-c0	Step 1	ENF without	44.2	
	Step 3	ENFR without	44.2	
	Step 4	ENFR propag	44.2	**57.8**
	Step 6	ENF without	**58.3**	
a45-R1.5-c0	Step 1	ENF without	44.9	
	Step 3	ENFR without	45.7	
	Step 4	ENFR propag	45.7	**55.7**
	Step 6	ENF without	**57.1**	

3.4   Energy Release Rate Curves

The determination of the crack length at any point of the test where P and δ are evaluated, allows the calculation of the energy release rate at any point during the crack propagation. The values of G_I and G_{II} have been obtained substituting the value of the crack length, in Eq.(3). As mentioned before, the corrected crack length a_I from Eq.(5) is applied to the determination of G_I. The R-curves obtained for some mixed mode tests can be seen in Fig. 10. Several specimens with different radius of the roller at different positions have been tested.
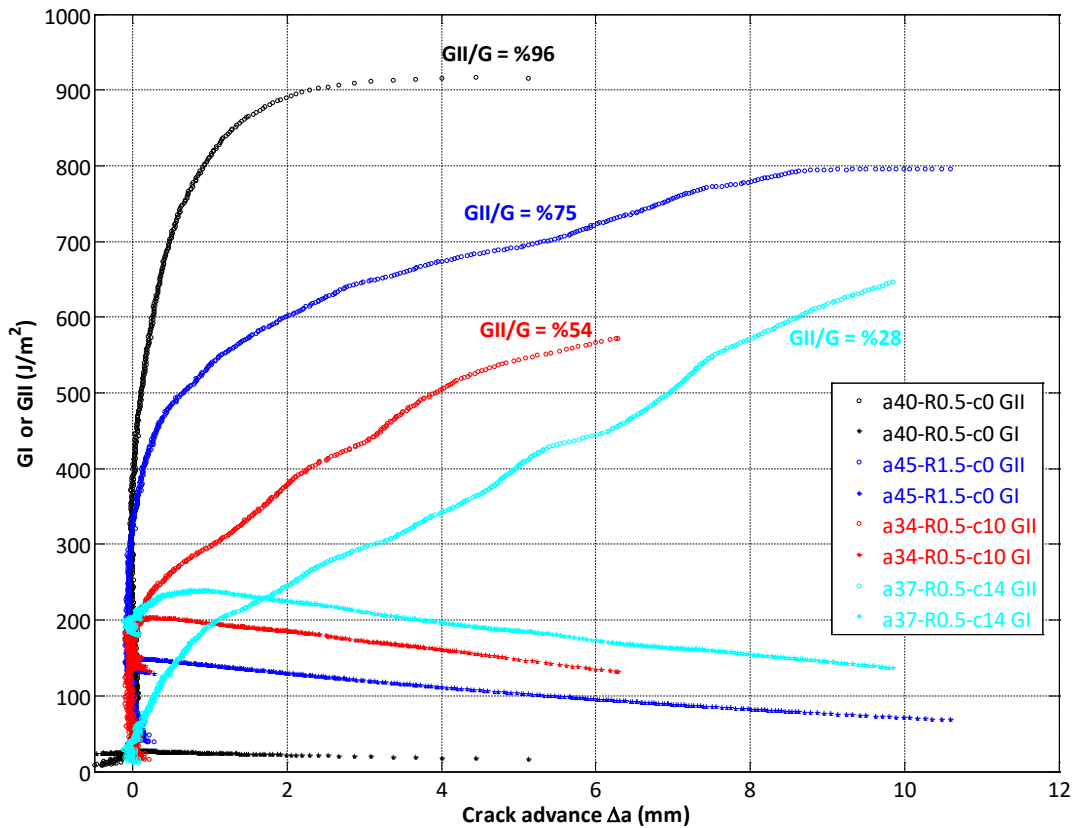
Fig. 10 R-curves for mixed mode tests

The upper curves correspond to G_{II}, and the lower ones to G_I. The curve of G_I and the curve of G_{II} that correspond to the same test configuration are drawn with the same color. When a propagates, the R-curves of G_I decrease slowly. At the same time, the R-curves for G_{II} increase. This means that mode ratio defined as G_{II}/G, is changing during the crack propagation. The initial values of energy release rate for each mode can be determined in the intersection of the curves with the vertical axis. As there is much data dispersion at that point, the initial value has been defined as Δa=0.25mm, considering it as non-linearity point. This assumption is supported by the fact that crack length is determined based on the variation of the compliance of the specimen, as it is shown in Fig. 8 . Consequently, it is assumed that the loss of linearity occurs at that crack advance. The maximum initial mode ratio obtained is 96% and the minimum is 28%, as it can be seen in Fig. 10.

In the proposal of the test, it was shown that all the range of mode ratios could be achieved [38]. Nevertheless, experimental difficulties for obtaining low mode ratios have appeared when trying to introduce bigger radius of the roller, or trying to introduce it deeper between the crack arms, because in the limit case, the crack opened without any load application. On the one side, great radius values in the outer side lead to geometric non-linearities. On the other side, the excessive introduction of the roller at the inner side of the crack lead to spontaneous crack advances. In order to obtain mixed modes, the

roller has been inserted above the support (c = 0) or at the inner side (c > 0) in all cases with a maximum radius of 1.5 mm.

As it can be seen in Fig. 11, when the mode II is predominant the total energy release rate tends to a plateau. When the mode I is more important (initial mode ratio of 28%), the total G continues increasing. Those trends agree qualitatively with the results obtained in R-curves of the pure modes concerning ENF and DCB tests, respectively: a plateau in ENF tests [42] and the increase of G in DCB tests for the same material [43].
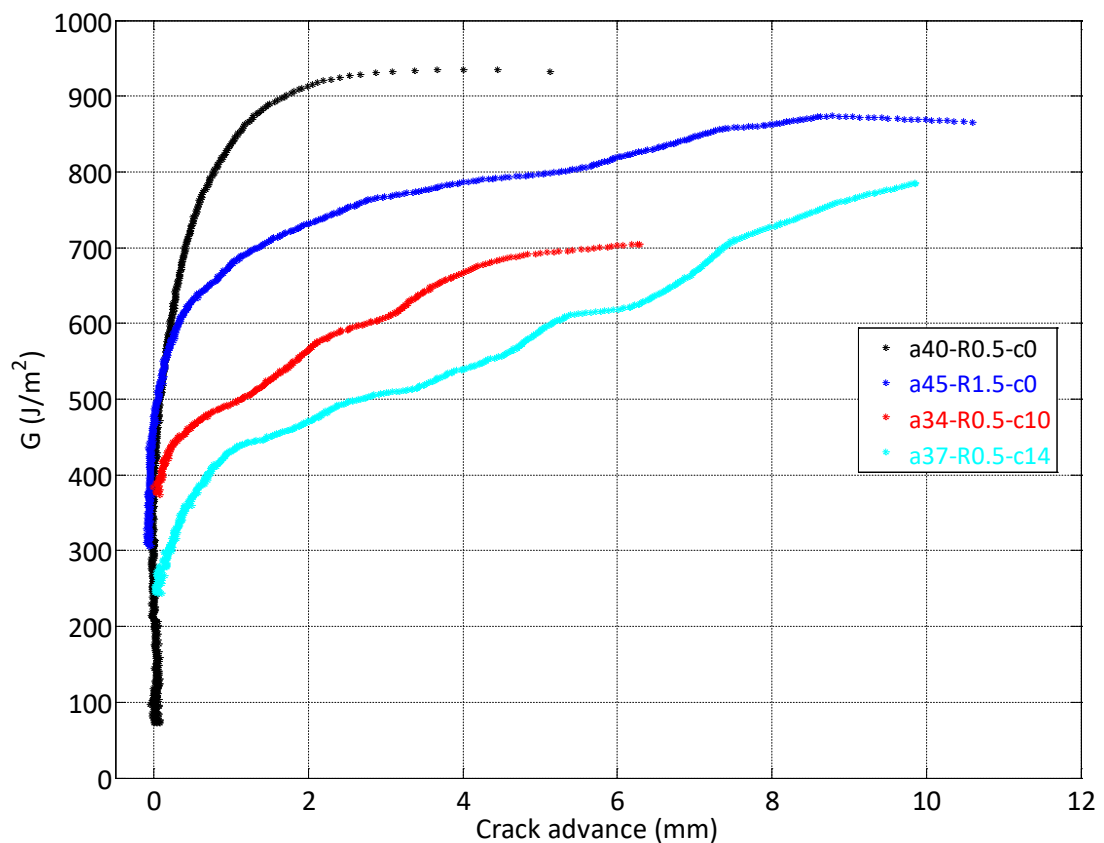
Fig. 11 Total energy release rate during propagation

Fig. 12 shows the change in mode ratio as a function of the crack advance. Therefore, it is possible to obtain in one test the evolution of the fracture toughness as a function of the mode ratio. Since the mode II increases and mode I decreases when the crack propagates, the mode ratio increases, as it is shown in Fig. 12.
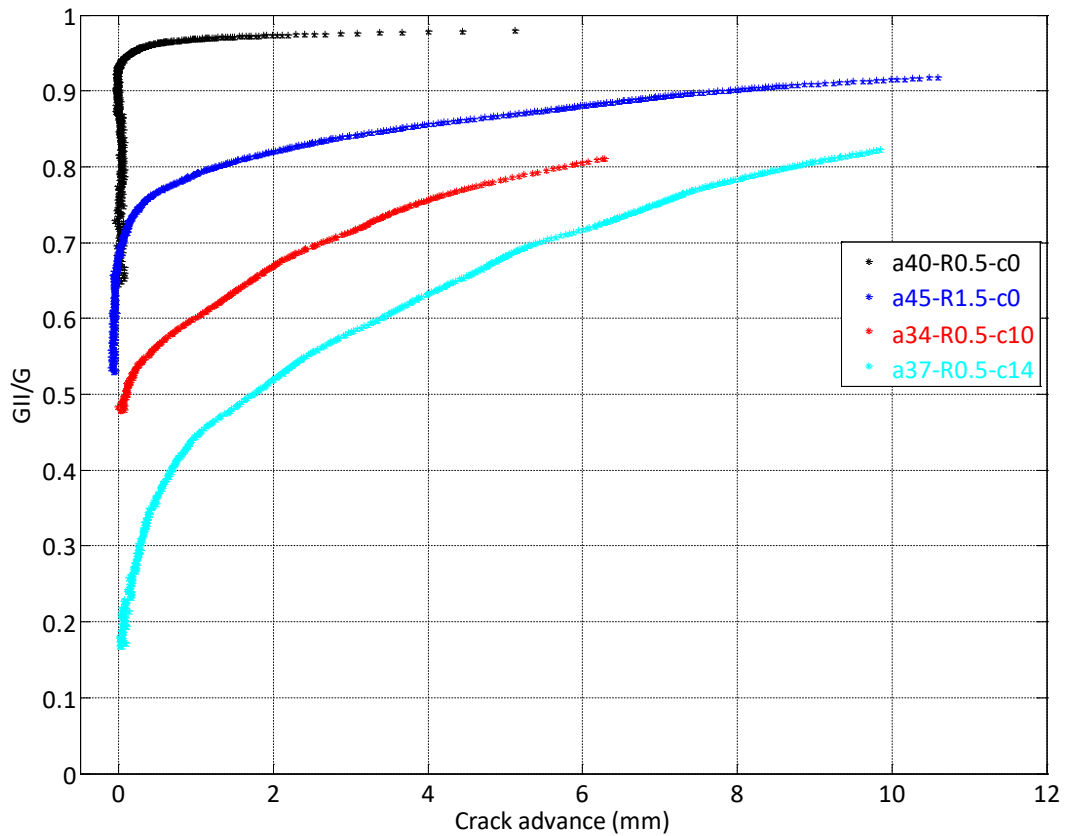
Fig. 12 Mode ratio during crack propagation

3.5   Determination of G_{Ic} and G_{IIc} by the linear criterion

A primary objective of characterising the laminate is to determine the locus for failure of G_I versus G_{II} [44,45]**.** Several mixed mode tests of different initial mode ratios have been analyzed, considering all the propagation data, for data reduction with the linear criterion [44]. To determine the initial mode ratio, the value of energy release rate for each mode contribution has been determined when Δa=0.25mm, as it was explained in section 3.4. As it can be seen in the load-displacement plot in Fig. 13, there are no load drops after the onset of the delamination thus the crack propagates in a stable manner. The initial mode ratio is 54% and the final mode ratio that corresponds to a crack advance of Δa = 6.2, mm is 81 %.
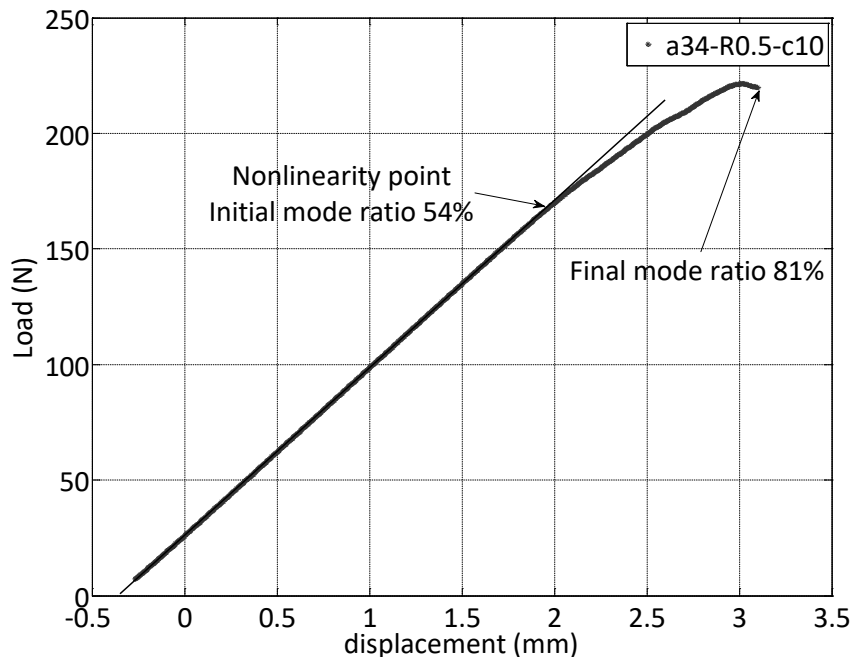
Fig. 13 Load displacement for mixed-mode test

As it is shown in Fig. 10, when the mode ratio is lower, the G_I curve has an initial tendency to rise and then after the maximum value, decreases monotonically. For instance, in the case of the initial mode ratio of 28% the decrease of G_I begins when $\Delta a = 0.85$ mm and the corresponding mode ratio at that point is 43%. Fig. 14 shows the data from the point where G_I starts to decrease in Fig. 10. The data corresponding to different mode ratio follow similar trend as the mode ratio changes during the test.
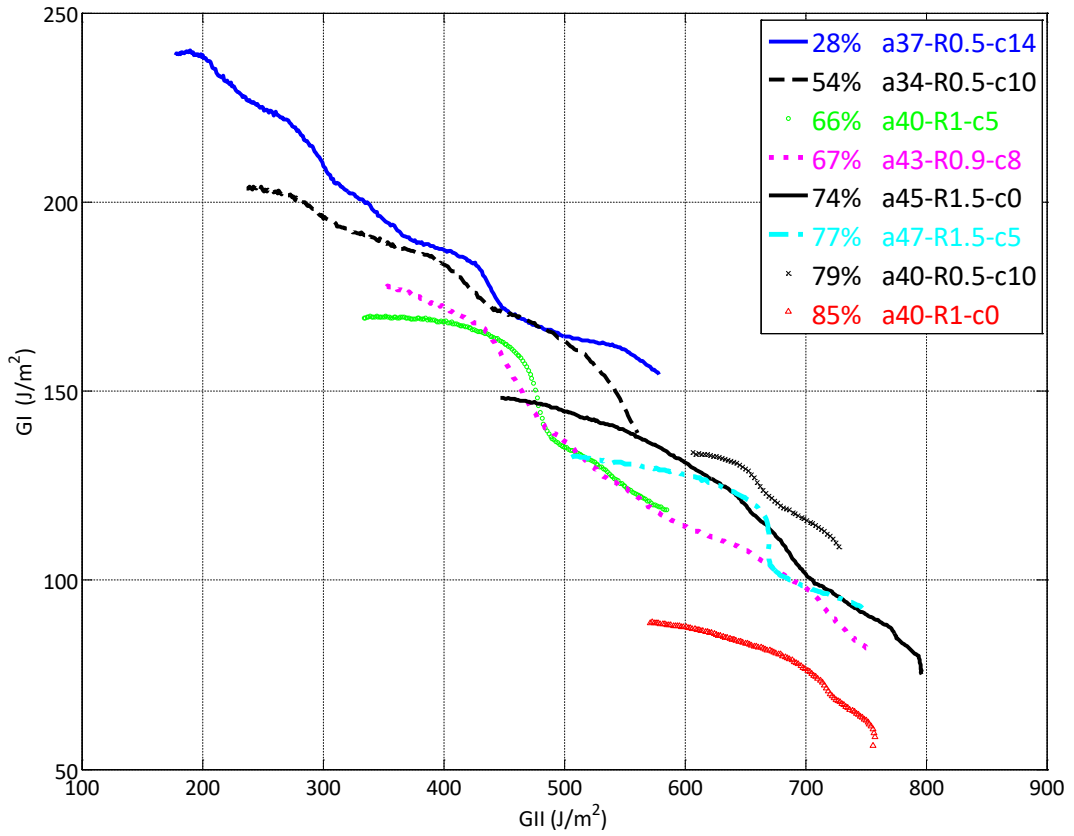
Fig. 14 Propagation data for different mode ratio

In order to evaluate the different fittings the *R* squared parameter has been determined as [46]:

$$R^2 = 1 - \frac{SS_{RES}}{SS_{TOT}}$$

$$SS_{RES} = \sum_{i}^{n} \left(G_{II\exp_i} - G_{II calculated_i} \right)^2 \qquad (9)$$

$$SS_{TOT} = \sum_{i}^{n} \left(G_{II\exp_i} - G_{II\exp AVERAGE} \right)^2$$

It is worth noting that the values of *R* squared parameter obtained using the expression of G_{II} are the same as those obtained using the expression of G_I. The results of linear fitting for initial mode ratios from 28% up to 85% can be found in Table 3.

Table 3 Linear fitting results for propagation

INITIAL MODE RATIO	Starting of G_I decrease MODE RATIO	FINAL MODE RATIO	G_{Ic} (J/m²)	G_{IIc} (J/m²)	R^2
28%	43%	82%	279	1251	0.983
54%	55%	81%	256	1328	0.961
66%	67%	83%	275	1012	0.892
66%	67%	90%	268	1071	0.977
74%	75%	91%	261	1159	0.965
77%	77%	89%	258	1154	0.860
79%	79%	87%	278	1198	0.969
85%	85%	93%	225	1045	0.991
		MEAN VALUE	**263 ± 16**	**1152 ± 100**	

According to the results of the R squared parameter, the linear criterion can be considered suitable for representing the propagation fracture toughness envelope. That result agrees with other published results [22]. Furthermore, it is worth noting that the standard deviation of values of G_{Ic} and G_{IIc} corresponding to 8 specimens is low.

Concerning the mode I fracture toughness, according to the standard [47], the recommended definition for determining G_{Ic} is the NL point. Observing the R-curve of DCB test for this material [43], the value of G_{Ic} that correspond to NL point is 240 J/m². This agrees with the result for mode I fracture toughness obtained in Table 3.

Regarding mode II, according to the standard [41], G_{IIc} is obtained based on the maximum load point of the load-displacement graph. Fig. 15 shows the R-curves corresponding to 5 specimens that have been tested in ENF configuration at a span of 120 mm following the BTBR method. The mean value for G_{IIc} determined in the maximum load point has been G_{IIc} =1063 J/m², which agrees with the result obtained in Table 3.
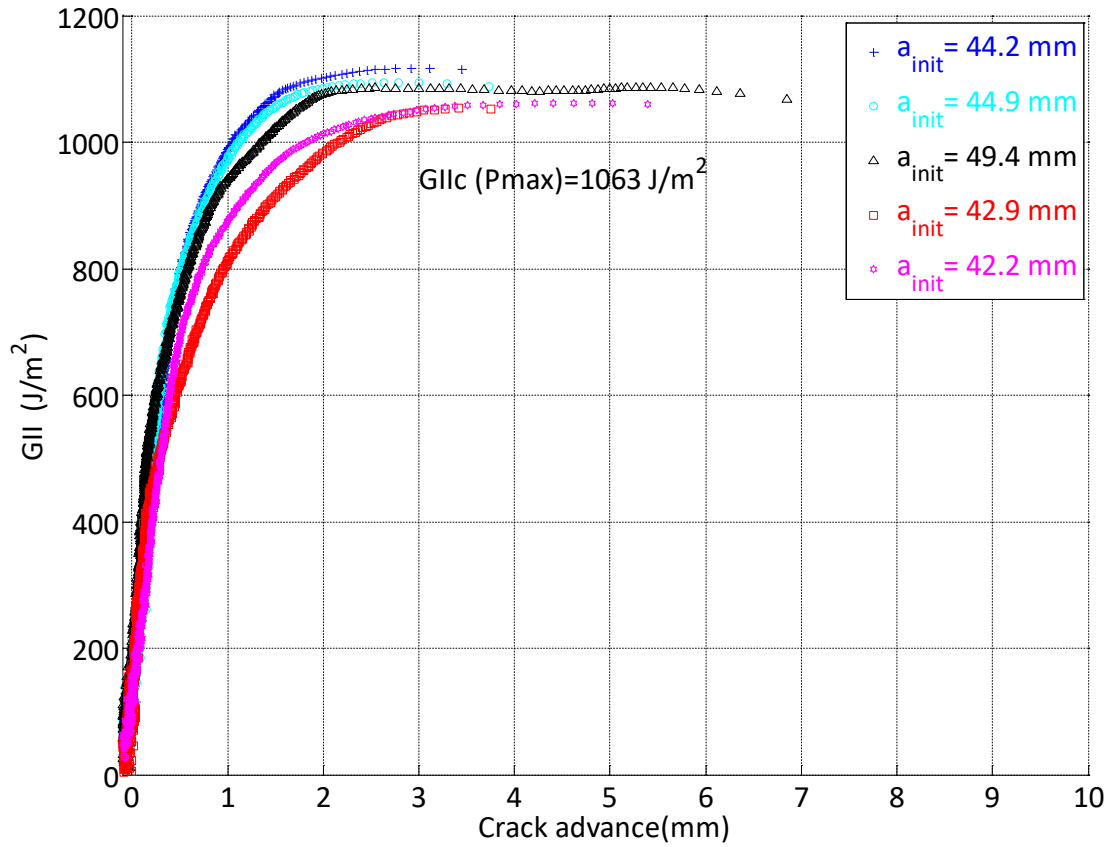
Fig. 15 ENF tests for determining G_{IIc}

Therefore, with one mixed-mode fracture test it is possible to find values for G_{Ic} and G_{IIc}, after having checked the suitability of the linear criterion based on pure mode tests.

As linear criterion is adopted, it results:

$$\frac{G_I}{G_{Ic}} + \frac{G_{II}}{G_{IIc}} = 1 \tag{10}$$

Analyzing the direct contribution of each mode to failure, each normalized mode ratio can be defined as:

$$\frac{G_I}{G_{Ic}} = G_I^{\,0} \qquad \qquad \frac{G_{II}}{G_{IIc}} = G_{II}^{\,0} \tag{11}$$

In Fig. 16 the propagation data from Fig. 14 are represented in terms of normalized mode ratios from Eq (11). The straight line is the representation of the linear criterion that corresponds to the mean values of Table 3.
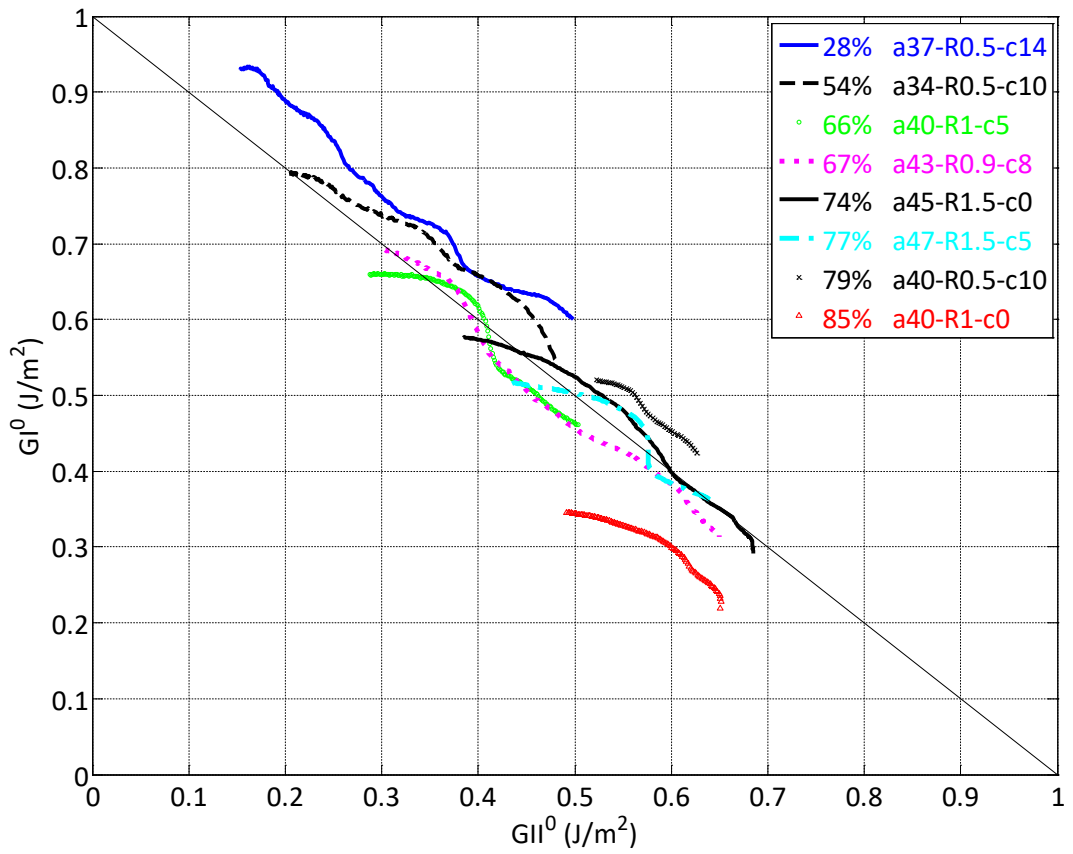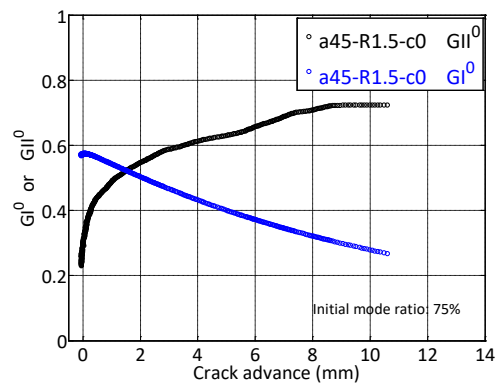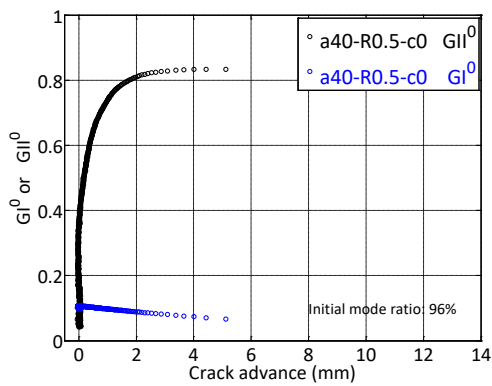
Fig. 16 Propagation data. Normalized mode ratios

The R-curves shown in Fig. 10 have been plotted in Fig. 17 in terms of the normalized mode ratios. For clarity, each test configuration has been plotted separately.
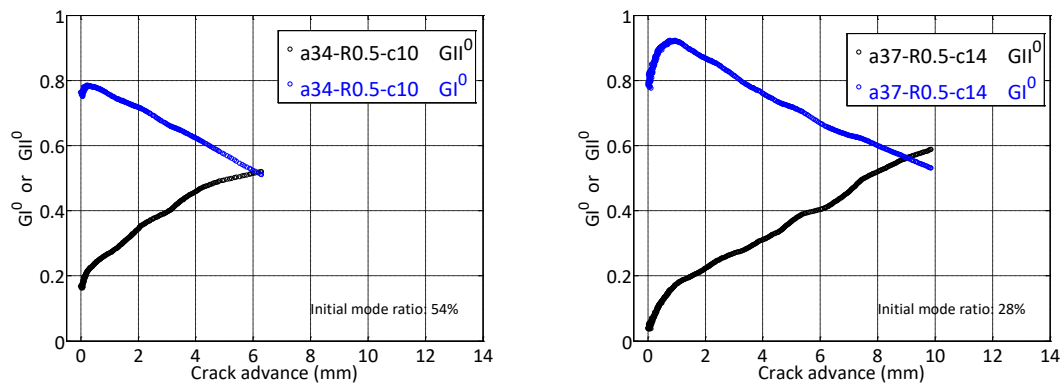
Fig. 17 Normalized energy release rates with respect to critical values

According to Fig. 17, when the mode II is clearly predominant, the G_{II}^0 curve is above the G_I^0 curve, as in the R curves. Nevertheless, for the initial mode ratio of 28%, the curve of G_I^0 is above the curve of G_{II}^0 during almost all the propagation, in contrast to what happened in R curves representation. Therefore, these normalized parameters describe better the weight of each mode in interlaminar fracture.

4   SUMMARY AND CONCLUSION

Mixed-mode I/II tests have been carried out by means of ENFR test configuration with specimens of F593/T 300 carbon/epoxy unidirectional composite.

Based on the variation of the compliance during the test, the crack length has been determined at any point through the whole test without any optical measurement. The suitability of the crack length determination has been checked by testing also the specimens in ENF configuration and applying the BTBR method.

The determination of the crack length has allowed the calculation of the energy release rate of each mode at every point of the crack propagation. As mode ratio changes during propagation, testing each specimen provides a set of values that correspond to increasing G_{II}/G mode ratio values.

The linear fracture criterion has been used for fitting experimental data of different specimens at different test conditions. On the one side the R squared parameter that indicates the quality of the linear regression, is greater than 0.86 in the eight cases analyzed. On the other side, the mean values of G_{Ic} and G_{IIc} obtained agree with those obtained from pure mode tests and the standard deviation values are low in both cases. Therefore, the linear criterion can be considered suitable for representing the propagation fracture toughness envelope in the material tested. In the case of any other material, ENFR

test can be considered as a complementary way for determining pure mode values G_{Ic} and G_{IIc}, provided that the linear criterion is satisfied.

5   REFERENCES

[1] Garg AC. Delamination—a damage mode in composite structures. Eng Fract Mech 1988;29:557-84.

[2] Friedrich K. Application of fracture mechanics to composite materials. : Elsevier, 1989.

[3] Hashemi S, Kinloch AJ, Williams JG. Mechanics and mechanisms of delamination in a poly(ether sulphone)—Fibre composite. Composites Sci Technol 1990;37:429-62.

[4] Sridharan S. Introduction. In: Sridharan S, editor. Delamination Behaviour of Composites: Woodhead Publishing; 2008, p. xxi-xxiii.

[5] Kinloch AJ, Wang Y, Williams JG, Yayla P. The mixed-mode delamination of fibre composite materials. Composites Sci Technol 1993;47:225-37.

[6] Charalambides M, Kinloch A, Wang Y, Williams J. On the Analysis of Mixed-Mode Failure. Int J Fract 1992;54:269-91.

[7] Anderson TL. Fracture mechanics :fundamentals and applications. 3rd ed. : CRC Press, 2005.

[8] Oden JT, Ripperger EA. Mechanics of elastic structures. 2nd ed. : McGraw-Hill etc., 1981.

[9] Raju IS, O'brien TK. 1 - Fracture mechanics concepts, stress fields, strain energy release rates, delamination initiation and growth criteria. In: Sridharan S, editor. Delamination Behaviour of Composites: Woodhead Publishing; 2008, p. 3-27.

[10] Brunner AJ, Blackman BRK, Davies P. A status report on delamination resistance testing of polymer–matrix composites. Eng Fract Mech 2008;75:2779-94.

[11] Pereira AB, de Morais AB. Mixed mode I + II interlaminar fracture of carbon/epoxy laminates. Composites Part A: Applied Science and Manufacturing 2008;39:322-33.

[12] Vandellos T, Hautier M, Carrere N, Huchette C. Development of a new fracture test to identify the critical energy release rate: The Tensile Flexure test on Notched Specimen. Eng Fract Mech 2012;96:641-55.

[13] Kim BW, Mayer AH. Influence of fiber direction and mixed-mode ratio on delamination fracture toughness of carbon/epoxy laminates. Composites Sci Technol 2003;63:695-713.

[14] Shahverdi M, Vassilopoulos AP, Keller T. Mixed-mode quasi-static failure criteria for adhesively-bonded pultruded GFRP joints. Composites Part A: Applied Science and Manufacturing 2014;59:45-56.

[15] Mollon V, Bonhomme J, Vina J, Argueelles A. Mixed mode fracture toughness: An empirical formulation for G(I)/G(II) determination in asymmetric DCB specimens. Eng Struct 2010;32:3699-703.

[16] Mohan J, Ivanković A, Murphy N. Mixed-mode fracture toughness of co-cured and secondary bonded composite joints. Eng Fract Mech 2015;134:148-67.

[17] Tracy GD, Feraboli P, Kedward KT. A new mixed mode test for carbon/epoxy composite systems. Composites Part A: Applied Science and Manufacturing 2003;34:1125-31.

[18] Rikards R, Buchholz F-, Wang H, Bledzki AK, Korjakin A, Richard H-. Investigation of mixed mode I/II interlaminar fracture toughness of laminated composites by using a CTS type specimen. Eng Fract Mech 1998;61:325-42.

[19] Bennati S, Fisicaro P, Valvo PS. An enhanced beam-theory model of the mixed-mode bending (MMB) test-Part I: Literature review and mechanical model. Meccanica 2013;48:443-62.

[20] Oliveira JMQ, de Moura MFSF, Morais JJL. Application of the end loaded split and single-leg bending tests to the mixed-mode fracture characterization of wood. Holzforschung 2009;63:597-602.

[21] de Moura MFSF, Oliveira JMQ, Morais JJL, Xavier J. Mixed-mode I/II wood fracture characterization using the mixed-mode bending test. Eng Fract Mech 2010;77:144-52.

[22] Yoshihara H. Initiation and propagation fracture toughness of solid wood under the mixed Mode I/II condition examined by mixed-mode bending test. Eng Fract Mech 2013;104:1-15.

[23] Anh PN, Stéphane M, Myriam C, Jean-Luc C. R-curve on Fracture Criteria for Mixed-mode in Crack Propagation in Quasi-brittle Material: Application for Wood. Procedia Materials Science 2014;3:973-8.

[24] da Silva LFM, Esteves VHC, Chaves FJP. Fracture toughness of a structural adhesive under mixed mode loadings. Materialwiss Werkstofftech 2011;42:460-70.

[25] Stamoulis G, Carrere N, Cognard JY, Davies P, Badulescu C. On the experimental mixed-mode failure of adhesively bonded metallic joints. Int J Adhes Adhes 2014;51:148-58.

[26] Chaves FJP, da Silva LFM, de Moura MFSF, Dillard DA, Esteves VHC. Fracture Mechanics Tests in Adhesively Bonded Joints: A Literature Review. J Adhesion 2014;90:955-92.

[27] Silva FGA, de Moura MFSF, Dourado N, Xavier J, Pereira FAM, Morais JJL et al. Mixed-mode I+II fracture characterization of human cortical bone using the Single Leg Bending test. Journal of the Mechanical Behavior of Biomedical Materials 2016;54:72-81.

[28] Blackman BRK, Williams JG. Crack length determination difficulties in composites-their effect on toughness evaluation. Int Conf Fract , ICF 2005;2:915-20.

[29] Szekrenyes A. Prestressed fracture specimen for delamination testing of composites. Int J Fract 2006;139:213-37.

[30] Sans D, Stutz S, Renart J, Mayugo JA, Botsis J. Crack tip identification with long FBG sensors in mixed-mode delamination. Compos Struct 2012;94:2879-87.

[31] Szekrenyes A, Uj J. Over-leg bending test for mixed-mode I/II interlaminar fracture in composite laminates. Int J Damage Mech 2007;16:5-33.

[32] ASTM D6671-01. Standard test method for mixed mode I-mode II interlaminar fracture toughness of unidirectional fiber-reinforced polymer matrix composites   2006.

[33] Blanco N. Variable mixed-mode delamination in composite laminates under fatigue conditions. 2004;Ph.D. thesis, Universitat de Girona.

[34] Mathews MJ, Swanson SR. Characterization of the interlaminar fracture toughness of a laminated carbon/epoxy composite. Composites Sci Technol 2007;67:1489-98.

[35] Marat-Mendes RM, Freitas MM. Failure criteria for mixed mode delamination in glass fibre epoxy composites. Compos Struct 2010;92:2292-8.

[36] Bui QV. A Modified Benzeggagh-Kenane Fracture Criterion for Mixed-mode Delamination. Journal of Composite Materials 2011;45:389-413.

[37] Liu Y, Zhang C, Xiang Y. A critical plane-based fracture criterion for mixed-mode delamination in composite materials. Composites Part B: Engineering 2015;82:212-20.

[38] Boyano A, Mollón V, Bonhomme J, De Gracia J, Arrese A, Mujika F. Analytical and numerical approach of an End Notched Flexure test configuration with an inserted roller for promoting mixed mode I/II. Eng Fract Mech 2015;143:63-79.

[39] Williams JG. End corrections for orthotropic DCB specimens. Composites Sci Technol 1989;35:367-76.

[40] Mujika F. On the effect of shear and local deformation in three-point bending tests. Polym Test 2007;26:869-77.

[41] ASTM D7905/D7905M-14 Standard Test Method for Determination of the Mode II Interlaminar Fracture Toughness of Unidirectional Fiber-Reinforced Polymer Matrix Composites. 2014.

[42] Arrese A, Carbajal N, Vargas G, Mujika F. A new method for determining mode II R-curve by the End-Notched Flexure test. Eng Fract Mech 2010;77:51-70.

[43] De Gracia J, Boyano A, Arrese A, Mujika F. A new approach for determining the R-curve in DCB tests without optical measurements. Eng Fract Mech 2015;135:274-85.

[44] Williams JG. The fracture mechanics of delamination tests. The Journal of Strain Analysis for Engineering Design 1989;24:207-14.

[45] Reeder JR. An evaluation of mixed-mode delamination failure criteria. NASA technical memorandum 104210 Langley Research Center, Hampton, VA 1992.

[46] Walpole RE, Myers RH, Myers SL, Ye KE. Probability & Statistics for Engineers &; Scientists. 9A ed. : Pearson Educación, 2012.

[47] ASTM D5528 – 01 Standard Test Method for Mode I Interlaminar Fracture Toughness of Unidirectional Fiber-Reinforced Polymer Matrix Composites. 2001.